

XAF1 promotes osteoclast apoptosis by antagonizing the XIAP-caspase axis

Mingchao Zhang^{a,b,1}, Yingkang Huang^{b,1}, Jinyu Bai^{a,1}, Wushuang Xu^{a,1}, Huajian Shan^a, Lei Sheng^a, Xiang Gao^a, Yu Han^b, Shiyong Wang^b, Chaowen Bai^a, Bo Tian^a, Yichao Ni^a, Qirong Dong^{a,**}, Feng Ma^{b,***}, Xiaozhong Zhou^{a,*}

^a Department of Orthopedics, the Second Affiliated Hospital of Soochow University, Suzhou, 215004, Jiangsu, China

^b National Key Laboratory of Immunity and Inflammation, and Key Laboratory of Synthetic Biology Regulatory Elements, Suzhou Institute of Systems Medicine, Chinese Academy of Medical Sciences & Peking Union Medical College, Suzhou, 215123, Jiangsu, China

ARTICLE INFO

Keywords:

Apoptosis
Osteoclast
Osteolysis
Osteoporosis
XAF1

ABSTRACT

Background: Over-activated osteoclast (OC) is a major cause of diseases related to bone loss and bone metabolism. Both bone resorption inhibition and apoptosis induction of osteoclast are crucial in treating these diseases. *X-linked inhibitor of apoptosis protein (XIAP)-associated factor 1 (XAF1)* is an important interferon-stimulated and apoptotic gene. However, how *XAF1* regulates bone formation and remodeling is unknown.

Methods: We generate global and chimeric *Xaf1* knockout mouse models and utilize these models to explore the function and mechanism of *XAF1* in regulating bone formation and remodeling *in vivo* and *in vitro*.

Results: We show that *XAF1* depletion enhances osteoclast generation *in vitro*. *XAF1* knockout increases osteoclast number and bone resorption, thereby exacerbating bone loss in both OVX and osteolysis models. Activation of *XAF1* with BV6 (a potent XIAP inhibitor) suppresses osteoclast formation. Mechanistically, *XAF1* deletion decreases osteoclast apoptosis by facilitating the interaction between XIAP and caspase-3/7.

Conclusions: Our data illustrates an essential role of *XAF1* in controlling osteoclastogenesis in both osteoporosis and osteolysis mouse models and highlights its underlying mechanism, indicating a potential role in clinical treatment.

The translational potential of this article: The translation potential of this article is that we first indicated that osteoclast apoptosis induced by *XAF1* contribute to the progression of osteoporosis and osteolysis, which provides a novel strategy in the prevention of osteoporosis and osteolysis.

1. Introduction

Osteoporosis is a common disease that causes fragility fractures as a result of a systemic deterioration of bone mass and microarchitecture. The medical and socioeconomic costs of osteoporosis in general, and postmenopausal osteoporosis in particular, will increase further as the population ages [1]. Bone turnover is a strictly controlled process in the physiologic steady state where the rate of osteoclast-mediated bone resorption and osteoblast-mediated bone formation are in balance [2]. Across a variety of osteoporosis types, decreased bone resorption provides a positive bone balance for osteoporosis treatment [3].

Mounting evidences indicate that bone is an immune regulatory organ and factors once thought to be immune system-related significantly affect bone health and disease [4–6]. OCs are multinucleated cells differentiated from bone marrow-derived macrophages (BMMs), which are a subset of the innate immune system [7,8]. Immune system B cells produce antibodies and RANKL to directly stimulate OC precursors [9] and T cells suppress the generation of OCs to lessen bone loss [10]. Interferons (IFN) have been reported to be essential for a variety of immunological responses, such as the stimulation of anticancer activity [11], which are also involved in OCgenesis. IFN- α inhibits the formation of OCs via preventing c-Fos expression and IFN- β exerts inhibitory

* Corresponding author. 1055 Sanxiang Road, Department of Orthopedics, The Second Affiliated Hospital of Soochow University, Suzhou, Jiangsu. China.

** Corresponding author.

*** Corresponding author. 100 Chongwen Road, Suzhou Institute of Systems Medicine, Chinese Academy of Medical Sciences & Peking Union Medical College, Suzhou, Jiangsu, China.

E-mail addresses: dongqirong@suda.edu.cn (Q. Dong), maf@ism.pumc.edu.cn (F. Ma), zhouxz@suda.edu.cn (X. Zhou).

¹ These authors contributed equally to this work.

effects on OCgenesis via JAK1/STAT3/c-Fos signaling [12,13], indicating IFN signaling is involved in OCs.

X-linked inhibitor of apoptosis (XIAP) associated factor 1 (*XAF1*) was identified as a novel IFN-stimulated gene (ISG) by Leaman et al., in 2002 [14]. Both IFN- α and IFN- β increased the levels of *Xaf1* messenger RNA (mRNA) in WM9 cells [15]. Meanwhile *XAF1* is also concerned with IFN-induced apoptosis [16]. It acts as an antagonist of XIAP by restoring caspase activity that XIAP has inhibited [17]. The co-expression of *XAF1* and XIAP enhance nuclear translocation of XIAP and hinder XIAP-dependent caspase-3 inhibition, as demonstrated by the incubation of recombinant XIAP with caspase-3 in the absence or presence of *XAF1* [17,18]. Spontaneous apoptosis is required for OC longevity, which is associated with activation of the caspase downstream of the extrinsic and intrinsic complementary pathways [19,20]. It's of critical importance for us to understand osteoclast behavior during bone resorption and remodeling via OC apoptosis and its modulation [21]. Previous study has shown that OC apoptosis occurs among patients with osteoporosis [22]. Whether *XAF1* is involved in OCgenesis and OC apoptosis has been unclear. Therefore, it is crucial to clarify the role and mechanism of *XAF1* in OCs.

Here, we investigated the effect of *XAF1* on OCs by global deletion and bone marrow chimera during steady-state conditions in mouse models of chronic (OVX-induced osteoporosis) and acute (Ti-particle-induced osteolysis) bone loss. Mechanistically, we demonstrated that *XAF1* functions as osteoprotective regulator that increased and preserved bone mass in response to both chronic and acute conditions. This bone-protective effect of *XAF1* involved in a decrease in the expression of osteoclastic genes and amplification of OC apoptosis, rather than depended on a direct effect on bone-formation osteoblasts. *XAF1* deletion led to a robust interaction between XIAP and caspase. These findings implied that *XAF1* may serve as an osteoprotective regulator to restore bone homeostasis.

2. Materials and methods

2.1. Study approval

Human studies were approved by the Ethics Committee of the Second Affiliated Hospital of Soochow University. All participants have signed informed consent. All *in vivo* animal experimentations and protocols were approved by the Institutional Animal Care and Use Committee of Soochow University.

2.2. Mice

Xaf1^{-/-} mice with a C57BL/6N genetic background were generated by Cyagen Biosciences (Suzhou, China). In brief, a 4.4 kb chromosomal deletion on *Xaf1* (Gene ID: 327959) was generated by single guide RNAs (sgRNAs) 5'-TACAAGTTAGCTAGGGCTGTTGG-3' and 5'-TTCCGCTGTTCCAACGTGGTTGG-3'. Primers for genotyping mice identification were 5'-GATGGAATGGTTGGCAGCGTTC-3' (F1), 5'-CTCCTGACACTCATGGGATTG-3' (R1), and 5'-GTACCAGGGCAA CAGGCAACTTTC-3' (R2). PCR product sizes were 635 bp (F1+R1, WT mice) and 910 bp (F1+R2, *Xaf1*^{-/-} mice). WT C57BL/6N mice for *in vitro* experiments were purchased from Vital River Laboratory Animal Technology (Beijing, China). All the mice were kept in the specific pathogen-free (SPF) environment at Suzhou Institute of Systems Medicine (ISM) under a controlled temperature (25 °C) and a 12h day-night cycle. The Animal Service Center of ISM authorized all animal research in accordance with the US National Institutes of Health Guide for the Care and Use of Laboratory Animals. (ISM-IACUC-0011-R). For OVX model, 8-week-old female *Xaf1*^{-/-} mice and its littermates were anesthetized and underwent bilateral ovariectomy or sham operation. After 8 weeks, blood samples, femora and tibias were harvested for further study. For osteolysis model, 8-week-old male *Xaf1*^{-/-} mice and its littermates were anesthetized and implanted Ti particle (3 mg/mice) in

calvaria. After 2 weeks, blood samples and crania were harvested for further analysis.

2.3. Antibodies and other reagents

Rabbit primary antibodies against TRAP (catalog ab191406), MMP9 (catalog ab38898), c-Fos (catalog #2250), NFATc1 (catalog ab25916), GAPDH (catalog #2118), CTSK (catalog #19027), *XAF1* (catalog ab17204), XIAP (catalog #2042), Cleaved Caspase3 (catalog #9664), Caspase3 (catalog #14220), Cleaved Caspase7 (catalog #8438) and Caspase7 (catalog #12827) were purchased from Abcam and Cell Signaling Technology. Mouse primary antibodies against XIAP (catalog sc-55550), Caspase3 (catalog sc-56053) were purchased from Santa Cruz. HRP-linked secondary antibodies specific for rabbit IgG and mouse IgG were also from Cell Signaling Technology. XIAP antagonist BV6 was purchased from MedChemExpress.

2.4. Osteoclastogenesis assay

Bone marrow cells from hindlimbs (tibia and femur) were cleansed and red blood cell lysis buffer was used to remove erythrocytes. Attached bone marrow cells were cultured in minimal essential medium (α -MEM, Gibco) with 10 % FBS, macrophage colony-stimulating factor (MCSF, R&D system), and RANKL (R&D system) in 12-well plates after 16h. Every two days, culture media was replaced, and cells were observed for the emergence of large-size cells. Cells were stained for tartrate resistant acid phosphatase (TRAP) (Sigma-Aldrich) after 5–8 days of culture, and the quantity of osteoclasts was determined under microscope. As for bone resorption assay, mature osteoclasts went through ultrasonication after incubation in osteo assay surface (Corning) and resorption pits were observed with light microscope.

2.5. Osteogenesis assay

Bone marrow cells from hindlimbs (tibia and femur) were cleansed and red blood cell lysis buffer was used to remove erythrocytes. Cell suspensions were incubated with Dulbecco's modified Eagle's medium (DMEM) consisting of 50 μ M ascorbic acid sodium salt, 100 nM dexamethasone, and 10 mM beta-glycerophosphate (Sigma). ALP assay was performed after 7 days, and Alizarin red S staining was performed after 21 days as per manufacturer's protocol.

2.6. Phalloidin staining

BMMs seeded on glass coverslips were stimulated with MCSF and RANKL for 5–8 days. Cells were washed briefly with PBS, fixed in 4 % paraformaldehyde, permeabilized with 0.2 % Triton X-100 in PBS, and blocked with 5 % goat serum. Mature osteoclasts were detected by phalloidin staining (Beyotime Biotechnology) in accordance with instructions. Fluorescent signal was observed and photographed using the Leica TCS SP6 fluorescent microscope. The number and area of actin ring was circled with dotted white line and calculated by ImageJ, followed by statistical significance in Graphpad 8.0.2.263.

2.7. RNA extraction and quantitative real-time PCR (RT-qPCR)

Total RNA was isolated from BMMs in the presence of RANKL using TRIzol reagent (ThermoFisher Scientific) according to the manufacturer's directions. Synthesis of cDNA was performed using the PrimeScript RT Master Mix (Takara). TB Green Premix Ex Taq (Tli RNaseH Plus) was used for RT-qPCR amplification on a Roche LightCycler 480 II system. RT-qPCR primer sequences for target genes were listed in Table S1.

2.8. Western blot and immunoprecipitation (IP)

Proteins were extracted from BMMs in the presence of MCSF and RANKL for specific days. For western blot analysis, proteins were extracted from BMMs using RIPA lysis buffer (Beyotime Biotechnology) supplemented with protease inhibitor cocktail (Roche) and phosphatase inhibitor PhosSTOP (Roche) according to the manufacturer's instructions. Protein concentrations of the extracts were determined by bicinchoninic acid (BCA) assay (Beyotime Biotechnology) and adjusted with lysis buffer for equalization. Equal portions of protein extracts were loaded to SEMS-PAGE, transferred to polyvinylidene difluoride (PVDF) membranes (Millipore), and then blotted with the chemiluminescence horseradish peroxidase (HRP) substrate (Millipore). For IP, BMM protein extractions were lysed with lysis buffer (50 mM Tris-HCl, pH 7.5, 150 mM NaCl, 1 mM EDTA, and 1 % Triton X-100), followed with protein concentration quantification. A total of 500 µg protein lysates was incubated overnight with Protein A-agarose beads (Sigma-Aldrich) plus appropriate antibodies. Fusion proteins were eluted from the agarose and performed with western blotting.

2.9. Micro-computed tomography (µCT) analysis

Femurs and calvariae were scanned with a SkyScan 1176 scanner (Bruker, Aartselaar, Belgium) and raw data was obtained, following the general guidelines used for assessment of bone microarchitecture in rodents using µCT. Briefly, scanning was conducted at 50 kV, 200 µA using a 0.5-mm aluminum filter, at a resolution of 9 µm/pixel. Reconstruction of sections was achieved using the NRECON software (Bruker) with beam hardening correction set to 40 %. The analysis was performed on a volume of interest within 200 slides of the trabecular region of the femur. Morphometric quantification of bone indices such as trabecular (or cortical) bone volume fraction (BV/TV%), bone surface density (BS/TV%), trabecular number (Tb. N; 1/mm) and trabecular separation (Tb. Sp; mm) were performed using the CT analyzer program (Bruker). The three-dimensional imaging was performed using Mimics software (Materialise). The region of interest (ROI) selected for distal femora was 5 % of femoral length from 0.1 mm below the growth plate. The bone structures within this ROI were then automatically classified using an algorithm.

2.10. Bone histology

Femur and calvaria specimens were harvested from mice operated with OVX or osteolysis and fixed in 4 % paraformaldehyde for 24 h at 4 °C. After demineralization in EDTA (10 %) for 20 days, specimens were dehydrated in graded concentrations of ethanol and embedded in paraffin. The serial sections (5 µm) were obtained with a microtome for H&E and TRAP staining.

2.11. TUNEL assay

BMMs were stimulated with RANKL for 3 d and harvested after fixation, rinsing and permeabilization. Apoptosis was detected using a TdT-mediated dUTP-digoxigenin nick-end labeling (TUNEL) assay, which specifically labeled the 3'-hydroxyl terminal of DNA strand breaks, according to the manufacturer's instructions.

2.12. Flow cytometry

BMMs were pretreated with RANKL for 3 d and prepared as a single cell suspension for staining. For analysis of apoptosis, cell suspension was performed by Annexin V-FITC and PI apoptosis detection kit (BD Biosciences) according to the manufacturer's instructions. Data were obtained by a flow cytometer (LSR Fortessa, BD Biosciences) and analyzed by FlowJo™ (BD Biosciences).

2.13. In situ proximity ligation assay (In situ PLA)

Duolink *in situ* PLA (Duolink Detection kit) was used to detect interactions between XIAP and caspase-3. Briefly, BMMs plated on glass coverslips in the presence of RANKL (50 ng/mL) for 3 d were fixed using 4 % formaldehyde. The fixed cells were incubated with mouse anti-caspase3 and rabbit anti-XIAP primary antibodies. Each of the primary antibodies was given oligonucleotide-labeled secondary antibodies (PLA probes) by the Duolink system, which combined with a DNA amplification-based reporter system to generate a signal only when the two primary antibodies were sufficiently near to one another. The signal from each detected pair of primary antibodies was visualized as a spot according to the manufacturer's instructions. Slides were evaluated using a LEICA TCA SP8 confocal microscope.

2.14. Bone marrow transplantation

8-week-old C57BL/6J mice were selected as donors and recipients. Before bone marrow transplantation, CD45.1 positive receptor mice were irradiated at a high dose (800 rad, 8 Gy) for endogenous hematopoietic cell ablation. WT/*Xaf1*^{-/-} mice with CD45.2 were selected as donors for BMMs (extraction described as above). Bone marrow single cell suspension were injected through the tail vein into the receptor after MACS sorting for myeloid cell line. Recombinant bone marrow chimera mice were kept in a SPF environment. After 8 weeks, chimera mice were performed OVX and Ti-particle implantation model for further study.

2.15. RNA-seq analysis

Total RNA was extracted from mice bone specimens without bone marrow and then subjected to cDNA synthesis by reverse transcription, followed by synthesis of biotinylated cRNA through *in vitro* transcription. Qubit 2.0 Fluorometer (Thermo Fisher Scientific) was used to detect the concentration of RNA samples. According to the instructions of the Agent 2100 bioanalyzer, samples were added to evaluate the integrity of the RNA. Ribosomal RNA Removal Kit (TruSeq Stranded mRNA Sample Prep Kit, Illumina) was used to construct the database and Illumina HiSeq*10 high-throughput analyzer was performed for RNA-Seq sequence. Adapter sequence was removed from raw data by CLC Genomics Workbench 12 (Qiagen), and all the samples were standardized by mouse mm10 reference genome for gene expression (RPKM, Reads Per Kilobase per Million mapped reads). CLC was also used to detect the difference in gene expression based on the p-value and fold change (p -value < 0.05, FC ≥ 2). Finally, these differentially expressed genes were analyzed by Gene Ontology or KEGG pathway functions.

2.16. Caspase-3 activity detection

Caspase-3 activity was measured spectrophotometrically via the detection of pNA cleavage from caspase-3-specific substrates. These experiments were completed using a caspase-3 assay kit (Beyotime). After cell lysates were incubated with Ac-LEVD-pNA for 2 h at 37 °C, the samples were read at 405 nm.

2.17. ELISA

Mouse serum was collected from the extracted eyeball blood. Blood samples were clotted for 30 min at room temperature and stored at 4 °C for 30 min. The samples were centrifuged at 3000 g and 4 °C for 10 min to obtain the serum. The concentrations of P1NP was measured with an ELISA kit (Signalway Antibody). RANKL and OPG were examined using another ELISA kit (R&D). All analyses were done in accordance with the manufacturers' instructions.

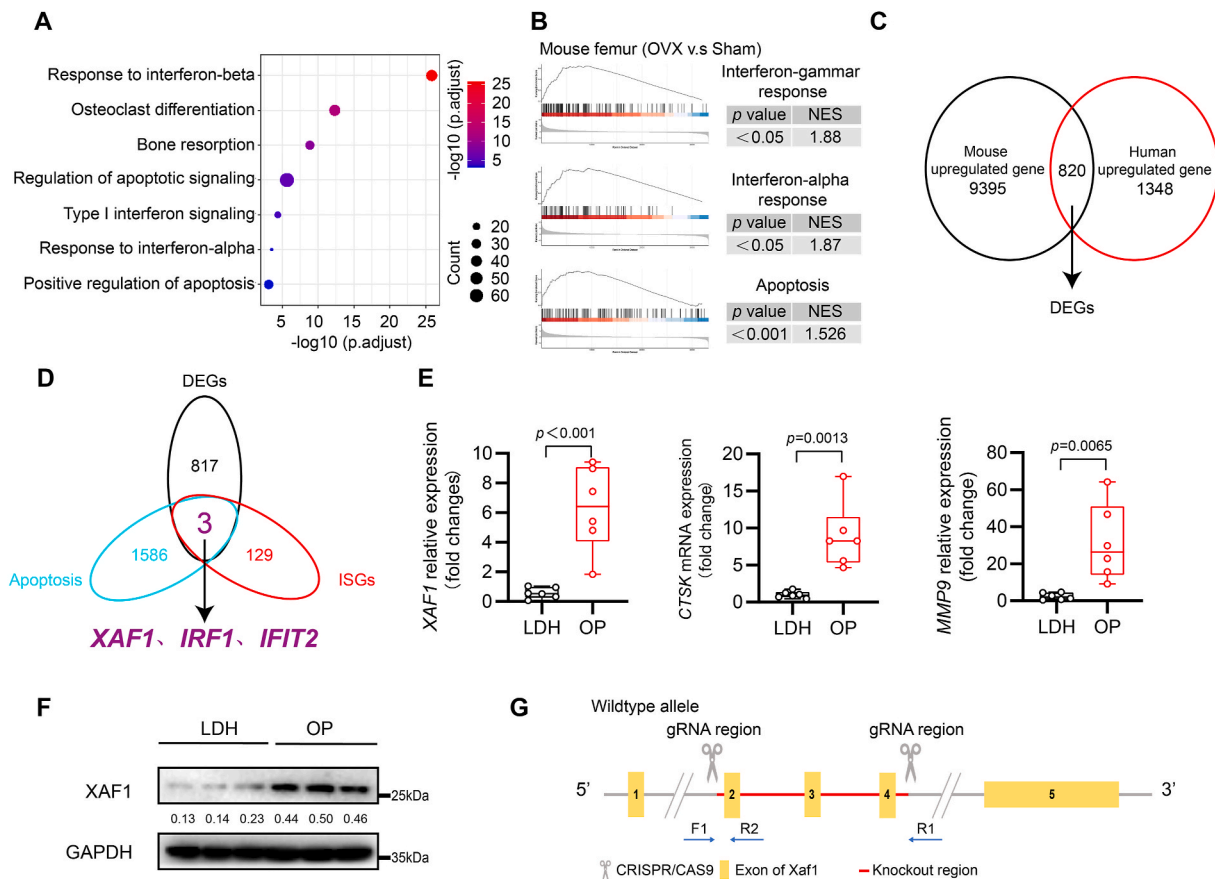


Figure 1. *XAF1* is upregulated in both osteoporotic patients and OVX mice. (A) Analysis of enriched KEGG pathways of significantly differentially expressed genes between OVX versus sham isolated femurs. (B) GSEAs showing upregulated genes belonging to the IFN and apoptosis signaling gene sets in OVX compared to sham isolated femurs. Enrichment score (ES) and normalized ES (NES) are shown. P -values < 0.05 was considered significant. (C) Schematic diagram of overlapped differentially expressed genes (DEG) between mouse and human upregulated genes. (D) Schematic diagram of overlapped genes among DEGs, IFN-stimulated genes (ISG) and apoptosis genes. (E) RT-qPCR analysis of *XAF1* and osteoclast-specific genes mRNA expression of the bone specimens of patients with lumbar disc herniation (LDH, control group, patients with normal BMD, $n = 6$) and osteoporosis (OP, patients with low BMD, $n = 6$). Data are shown as mean \pm SEM. (Student's t -test). (F) Western blot analysis of whole cell lysates from bone specimens of patients with lumbar disc herniation (LDH, control group, patients with normal BMD, $n = 3$) and osteoporosis (OP, patients with low BMD, $n = 3$). GAPDH is shown as a loading control. Data are representative of three independent experiments. (G) Schematic diagram of generation of *Xaf1* global deletion mice by using CRISPR-Cas9.

2.18. Statistical analysis

P values were calculated using One-way ANOVA with Holm-Sidak's multiple comparison test or unpaired Student's t -test in GraphPad Prism 8 software. All values are shown as the mean \pm SEM. Results are presented as representative examples of more than three independent experiments. Statistical tests were justified as appropriate for the results presented and the data met the assumptions of the tests.

3. Results

3.1. *XAF1* was increased in both osteoporotic patients and OVX mice

To explore the specific gene in OCgenesis and osteoporosis process, RNA-seq was performed between OVX and sham mice. Notably, pathway enrichment analysis of these genes revealed significant enrichment for the OC differentiation, IFN signaling and apoptosis, which are essential for OC function and survival (Fig. 1A). Meanwhile, among all the differentially expressed genes (DEGs) in the femurs treated with OVX, IFN and apoptosis signaling were highly and significantly enriched (Fig. 1B). To further explore the common target for osteoporosis both in human and mice, data from the Gene Expression Omnibus (Data ref: GSE230665, 2023) was utilized to overlap with data from mice, demonstrating 489 DEGs in common (Fig. 1C). In the view of

the significance of apoptosis and IFN, we next overlap DEGs with interferon-stimulated genes and apoptosis genes, *XAF1*, *IFIT2* (Interferon-Induced Protein with Tetratricopeptide Repeats 2) and *IRF1* (Interferon Regulatory Factor 1) were screened out (Fig. 1D). The intimate connection between *XAF1*, *IFIT2* and *IRF1* expression and OC function prompted us to explore the pathological involvement of them in human osteoporosis. We obtained bone specimens from patients with osteoporosis (OP) and normal bone mineral density (BMD). The source of bone specimens with normal BMD was lamina bone of young patients with lumbar disc herniation for laminectomy surgery. RT-qPCR was performed, indicating that *XAF1* increased with *ACP5* (Acid Phosphatase 5), *CTSK* (Cathepsin K) and *MMP9* (Matrix Metalloproteinase 9) in OP patients instead of *IRF1* and *IFIT2* (Fig. 1E–S1A). The expression of the *XAF1* protein in the OP group was higher than that in the control group (Fig. 1F). These data suggested that *XAF1* be closely associated with osteoporosis. Hence, *Xaf1* global knockout mice was generated as displayed (Fig. 1G) and knockout efficiency was presented by Western blot and RT-qPCR (Figs. S1B–C).

3.2. Global deletion of *Xaf1* promoted RANKL-induced osteoclastogenesis

To determine the influence of *Xaf1* targeting OCs, BMMs were isolated from WT and *Xaf1*^{-/-} mice and stimulated with RANKL for 7 days. Mature OCs were assessed by TRAP staining and bone resorption assay.

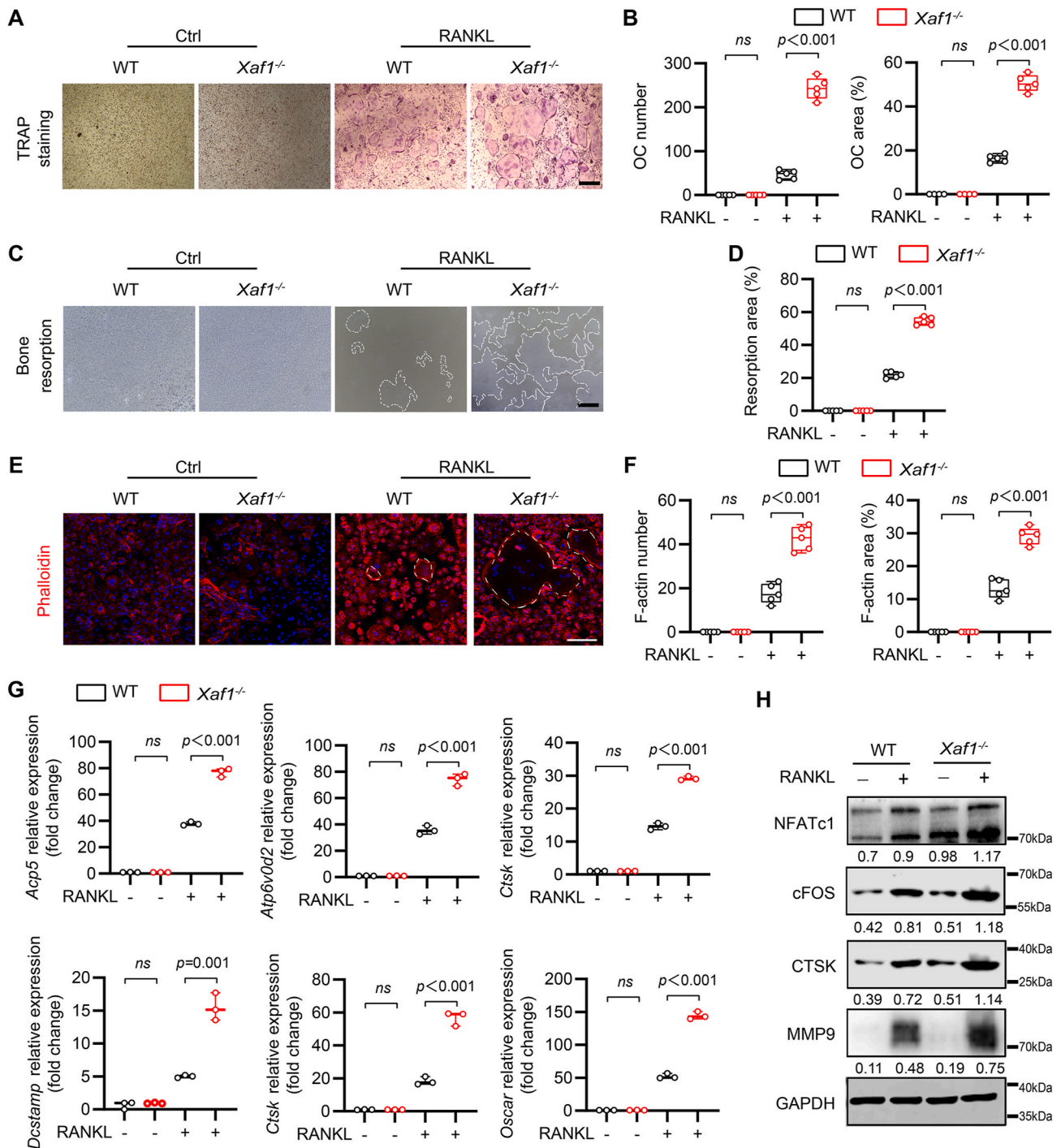


Figure 2. *Xaf1* deletion promotes RANKL-induced osteoclastogenesis. (A) Bone marrow cells isolated from WT and *Xaf1*^{-/-} mice were cultured on glass coverslips for 7 days in α -MEM medium supplemented with M-CSF (30 ng/ml) alone or with M-CSF and RANKL (50 ng/ml). On day 7, osteoclasts were stained with TRAP. Scale bar, 50 μ m. Data are representative of three independent experiments. (B) Quantification of osteoclast number and percentage of osteoclast area of (A). Data are shown as mean \pm SEM (Student's *t*-test). (C) Bone marrow cells isolated from WT and *Xaf1*^{-/-} mice were cultured on Osteo Assay surface for 7 days in α -MEM medium supplemented with M-CSF (30 ng/ml) alone or with M-CSF and RANKL (50 ng/ml). Representative images of resorption pits on Osteo Assay surface, scale bar, 100 μ m. Data are representative of three independent experiments. (D) Quantification of resorption pit area of (C). Data are shown as mean \pm SEM (Student's *t*-test). (E) Bone marrow cells isolated from WT and *Xaf1*^{-/-} mice were cultured on glass coverslips for 7 days in α -MEM medium supplemented with M-CSF (30 ng/ml) alone or with M-CSF and RANKL (50 ng/ml). On day 7, osteoclasts were stained with phalloidin. Representative images of fluorescence of cell nuclei and F-actin rings. Red, actin ring; blue, DAPI. Scale bar, 50 μ m. Data are representative of three independent experiments. (F) Quantification of F-actin rings and area of osteoclasts of (E). Data are shown as mean \pm SEM (Student's *t*-test). (G) RT-qPCR analysis of the osteoclast-specific genes mRNA expression of the BMM cultures isolated from WT (*n* = 3) and *Xaf1*^{-/-} mice (*n* = 3) incubated for 3 days with RANKL (50 ng/ml). Data are shown as mean \pm SEM (Student's *t*-test). (H) Western blot analysis of whole cell lysates from BMM cultures isolated from WT and *Xaf1*^{-/-} mice and stimulated with M-CSF (30 ng/ml) alone or with M-CSF and RANKL (50 ng/ml) for 3 days (*n* = 3). GAPDH is shown as a loading control. Data are representative of three independent experiments.

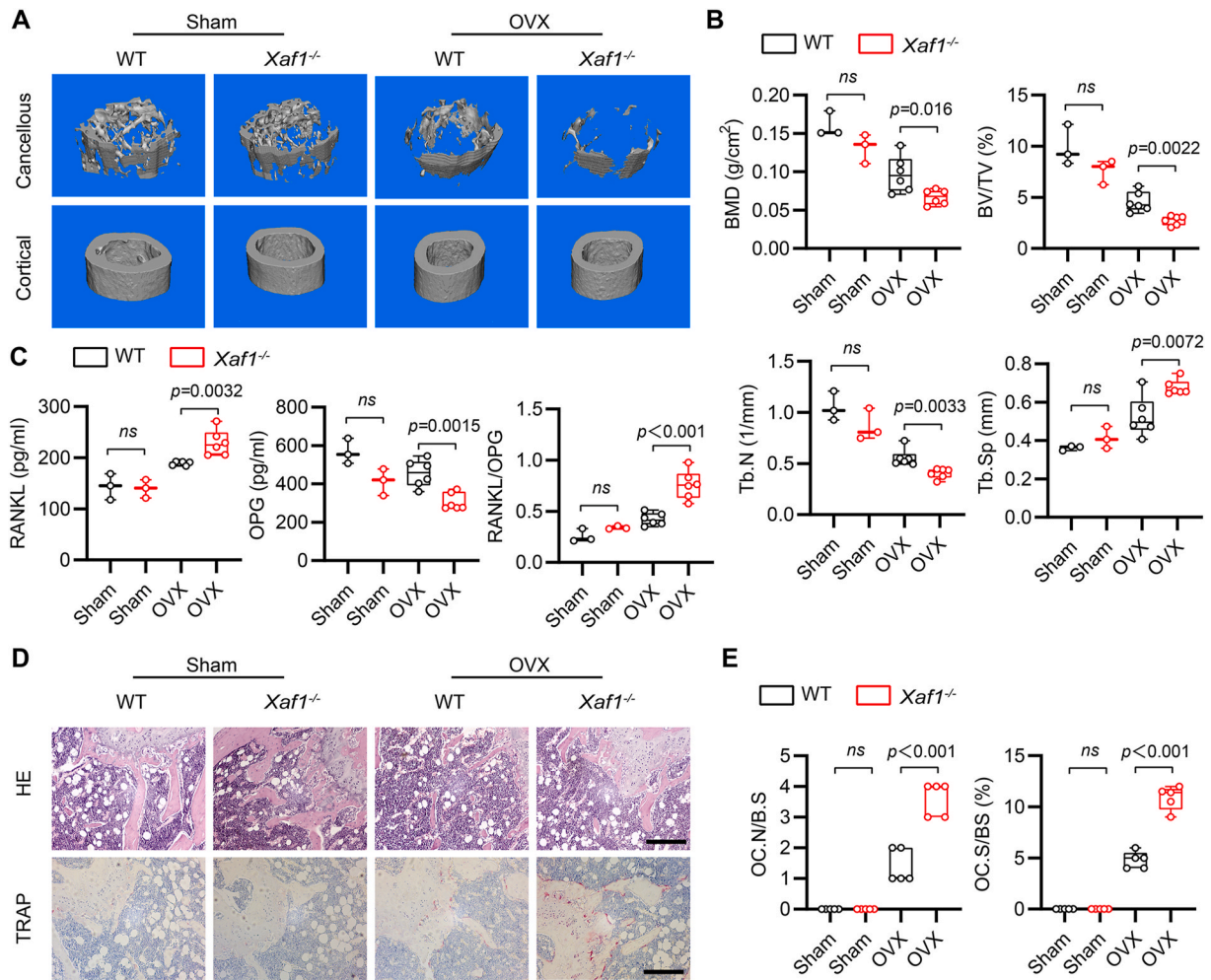


Figure 3. *Xaf1* deletion exacerbates OVX-induced bone loss *in vivo*. (A) Representative micro-CT pictures of hind legs of WT and *Xaf1*^{-/-} littermates after sham and OVX operation. Data are representative of three independent experiments. (B) Trabecular parameters, calculated on micro-CT scans of hind legs of WT and *Xaf1*^{-/-} littermates after sham and OVX operation. Each dot represents an individual mouse (Sham, n = 5; OVX, n = 6). Data are shown as mean ± SEM (One-way ANOVA between indicated genotypes). (C) Levels of RANKL and OPG in serum of WT and *Xaf1*^{-/-} littermates after sham and OVX operation. Each dot represents an individual mouse (Sham, n = 3; OVX, n = 6). Data are shown as mean ± SEM (One-way ANOVA between indicated genotypes). (D) Representative pictures of TRAP and H&E-stained sections from the femur of WT and *Xaf1*^{-/-} littermates after sham and OVX operation. Scale bar, 200 μm. (E) Quantification of the number and area of TRAP-positive cells on sections from the femur of WT and *Xaf1*^{-/-} littermates after sham and OVX operation. Data are shown as mean ± SEM (One-way ANOVA between indicated genotypes).

Xaf1^{-/-} BMMs formed more TRAP⁺ multinucleated OCs (Fig. 2A–B) and exhibited increased bone resorption capacity than BMMs derived from WT mice, manifested as increased number and area of OCs as well as more resorption pits and trails on the osteo surfaces (Fig. 2C–D). Consistent with results above, a striking size increase in actin ring structure was observed (Fig. 2E) and both the number of nuclei per osteoclast and actin rings per osteoclast were increased via phalloidin staining in *Xaf1*^{-/-} OCs (Fig. 2F). Moreover, a significant increase in the OC-specific gene expression, such as *Acp5*, *Oscar* (Osteoclast Associated Ig-Like Receptor), *Atp6v0d2* (ATPase H⁺ Transporting V0 Subunit D2), *Ctsk*, *Dcstamp* (Dendritic Cell-Specific Transmembrane Protein), and *Mmp9* were observed in *Xaf1*^{-/-} BMMs with RANKL stimulation (Fig. 2G). Subsequent western blot analyses of the key OC-specific markers NFATc1 (Nuclear Factor of Activated T cells 1), cFOS (Fos Proto-Oncogene), MMP9 and cathepsin K (CTSK) showed that RANKL induced the expression of all these markers, and *Xaf1* deletion augmented RANKL-induced expression of all markers compared with WT during OCgenesis (Fig. 2H).

ALP (Alkaline Phosphatase) (Figs. S2A–B) and alizarin red staining (Figs. S2C–D) were used to determine osteogenic activity, which demonstrated no difference between WT and *Xaf1*^{-/-} BMSCs. Likewise,

gene expression levels of a series of osteoblast markers, including *Runx2* (RUNX Family Transcription Factor 2), *Osterix* (known as Sp7 Transcription Factor), *Ocn* (Osteocalcin), and *Opn* (Osteopontin) were indistinguishable between WT and *Xaf1*^{-/-} BMSCs (Fig. S2E). Meanwhile, it's demonstrated that *Xaf1* depletion did not affect osteogenesis *in vivo* by ELISA and RT-qPCR (Figs. S2F–G). In summary, depletion of *XAF1* did not significantly affect osteoblast differentiation *in vitro* and *in vivo*. Together, these results indicated that *Xaf1* deletion selectively enhanced OC generation without affecting osteogenesis *in vitro*.

3.3. *Xaf1* deletion exacerbated OVX-induced bone loss *in vivo*

After establishing the cellular effects of *Xaf1* on OCs, we sought to define its role *in vivo*. OVX or sham surgeries were performed in 8-week old *Xaf1*^{-/-} mice and littermates. Reconstructed three-dimensional (3D) imaging was conducted using micro-computed tomography (μCT) (Fig. 3A). Interestingly, there was no significant difference between the bone mass of *Xaf1* knockout mice and that of wild-type mice at the physiological condition, which was consistent with previous studies demonstrating that *XAF1* expression was at low level under physiological conditions and only increased under the stimulation of

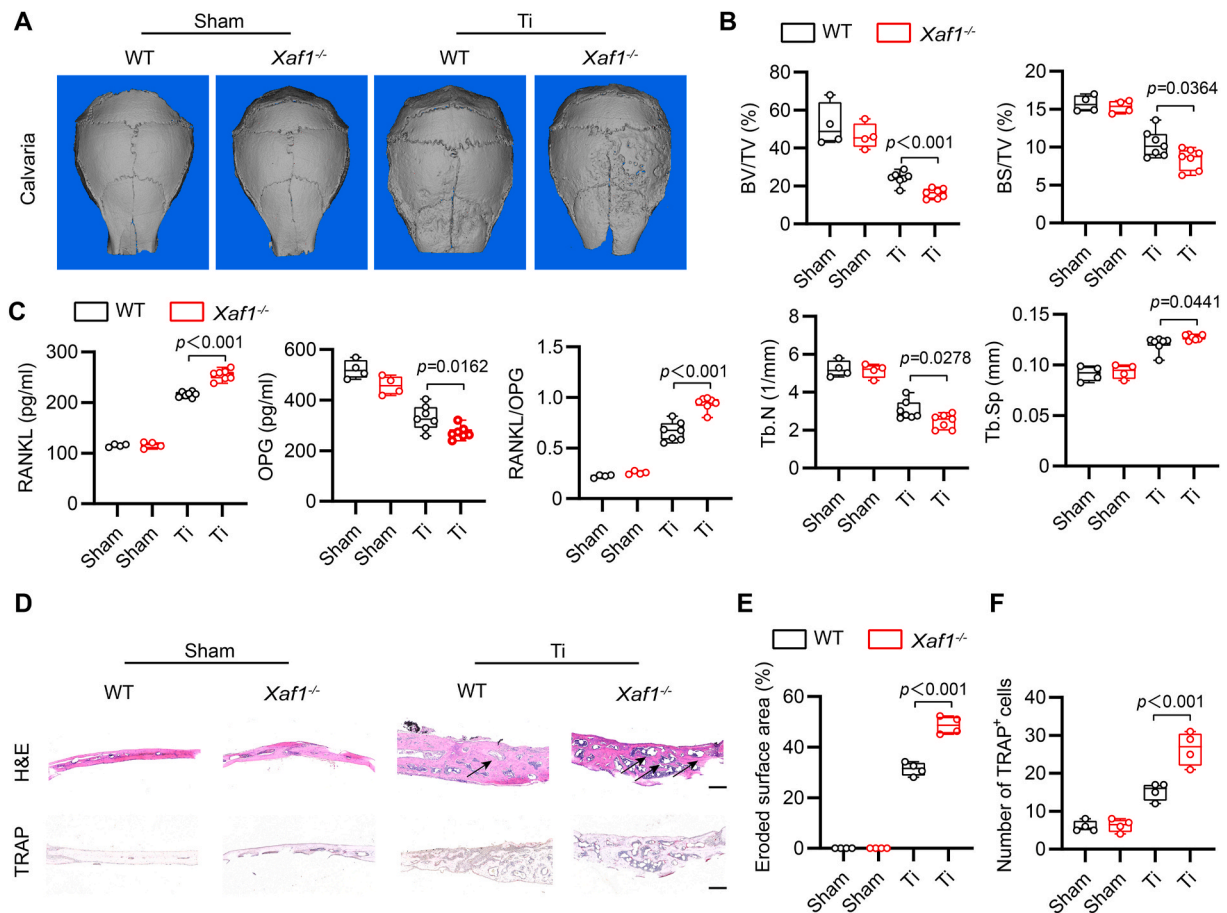


Figure 4. *Xaf1* deletion exacerbates Ti-particle induced osteolysis *in vivo*. (A) Representative micro-CT pictures of calvariae of WT and *Xaf1*^{-/-} littermates after sham and Ti particle implantation operation. Data are representative of three independent experiments. (B) Trabecular parameters, calculated on micro-CT scans of calvariae of WT and *Xaf1*^{-/-} littermates after sham and Ti particle implantation operation. Each dot represents an individual mouse (Sham, n = 4; Ti, n = 7). Data are shown as mean ± SEM (One-way ANOVA between indicated genotypes). (C) Levels of RANKL and OPG in serum of WT and *Xaf1*^{-/-} littermates after sham and Ti particle implantation operation. Each dot represents an individual mouse (Sham, n = 4; Ti, n = 7). Data are shown as mean ± SEM (One-way ANOVA between indicated genotypes). (D) Representative pictures of TRAP and H&E-stained sections from the calvariae of WT and *Xaf1*^{-/-} littermates after sham and Ti particle implantation operation (Sham, n = 4; Ti, n = 7). Data are representative of three independent experiments. Scale bar, 200 μm. (E) Quantification of the eroded surface area on sections from the calvariae of WT and *Xaf1*^{-/-} littermates after sham and Ti particle implantation operation. Data are shown as mean ± SEM (One-way ANOVA between indicated genotypes). (F) Quantification of the number of TRAP-positive cells on sections from the femur of WT and *Xaf1*^{-/-} littermates after sham and Ti particle implantation operation. Data are shown as mean ± SEM (One-way ANOVA between indicated genotypes).

inflammatory environment such as virus infection. OVX treated *Xaf1*^{-/-} mice revealed decreased bone mass, BMD, BV/TV, Tb.N, as well as increased Tb.Sp compared with OVX treated littermates (Fig. 3B).

Complementing these findings, serum was analyzed for the concentrations of RANKL, which promoted OCgenesis, and its regulatory decoy receptor OPG. *Xaf1* deletion significantly increased the RANKL/OPG ratio in blood serum (Fig. 3C). Elevated OC formation and bone resorption were often the underlying causes of low-bone mass osteoporotic phenotypes. In order to determine the number and activity of OCs, femur bone slices were stained with TRAP and H&E. As seen in Fig. 3D–E, femoral sections from *Xaf1*^{-/-} mice had higher numbers of OCs than littermates and exhibited low-bone mass osteoporotic phenotype in TRAP-stained and H&E-stained tissue samples, respectively. This observation revealed that *Xaf1* may have an osteoprotective impact in osteoporosis, which accounted for the decreased bone mass in *Xaf1*^{-/-} mice after OVX treatment.

3.4. *Xaf1* deletion exacerbated Ti-particle induced osteolysis *in vivo*

Osteolysis was an inflammatory bone loss caused by excessive OC formation and activity. Given the effect of *Xaf1* on noninflammatory osteoporosis, we considered if *Xaf1* conferred additional protection

during osteolysis. To induce osteolysis, Ti particles were injected onto the calvaria of *Xaf1*^{-/-} mice and littermates. It's demonstrated that XAF1 was increased after Ti-particle induction (Figs. S3A–B). Consistent with OVX model, the expression level of XAF1 under physiological conditions was insufficient to produce a distinct bone phenotype in osteolysis (Fig. 4A). μCT analysis revealed that the *Xaf1*^{-/-} mice exhibited a significant decrease in osteolysis compared to littermates (Fig. 4A). Morphological analysis revealed a significant reduction in BV/TV and an increase in the number of pores and the percentage of porosity from *Xaf1*^{-/-} mice compared to littermate mice (Fig. 4B). Serum levels of RANKL were upregulated from *Xaf1*^{-/-} mice, while OPG levels were comparable, resulting in the increase of RANKL/OPG ratio, a parameter for assessing OCgenesis (Fig. 4C). Collectively, these results indicated that *Xaf1* deletion exacerbated bone loss in Ti-particle-induced osteolysis.

Histological analysis was performed on calvarial sections to validate μCT results. H&E staining showed significant bone defects (Fig. 4D) and increased proportion of eroded surface in *Xaf1*^{-/-} mice (Fig. 4E). TRAP staining confirmed that the activity of osteoclasts along the surface of trabecular bone was higher in *Xaf1*^{-/-} mice than in littermates (Fig. 4D). Osteoclast number per bone perimeter (N.Oc/B.pm) was larger in *Xaf1*^{-/-} mice than in littermates (Fig. 4F). Together, these

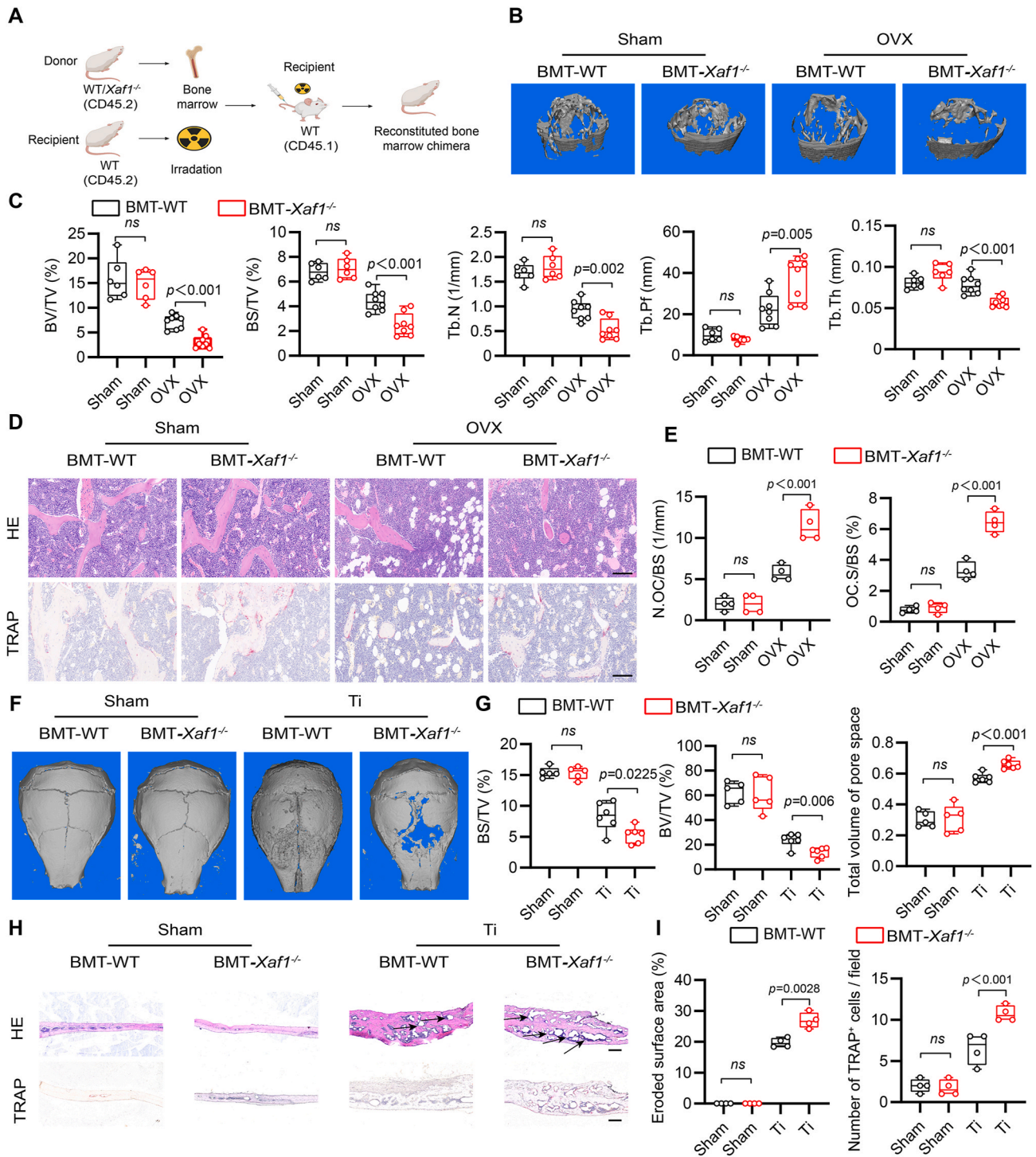


Figure 5. *Xaf1* deletion chimeras results in a low bone mass phenotype. **(A)** Schematic diagram of *Xaf1* chimera mice generation by bone marrow transplantation. **(B)** Representative micro-CT pictures of hind legs of chimeric WT and *Xaf1*^{-/-} littermates after sham and OVX operation. Data are representative of three independent experiments. **(C)** Trabecular parameters, calculated on micro-CT scans of hind legs of chimeric WT and *Xaf1*^{-/-} littermates after sham and OVX operation. Each dot represents an individual mouse (Sham, n = 6; OVX, n = 8). Data are shown as mean ± SEM (One-way ANOVA between indicated genotypes). **(D)** Representative pictures of TRAP and H&E-stained sections from the femur of chimeric WT and *Xaf1*^{-/-} littermates after sham and OVX operation. Data are representative of three independent experiments. Scale bar, 200 μm. **(E)** Quantification of the number and area of TRAP-positive cells on sections from the femur of chimeric WT and *Xaf1*^{-/-} littermates after sham and OVX operation. Data are shown as mean ± SEM (One-way ANOVA between indicated genotypes). **(F)** Representative micro-CT pictures of calvariae of chimeric WT and *Xaf1*^{-/-} littermates after sham and Ti particle implantation operation. Data are representative of three independent experiments. **(G)** Trabecular parameters, calculated on micro-CT scans of calvariae of chimeric WT and *Xaf1*^{-/-} littermates after sham and Ti particle implantation operation. Each dot represents an individual mouse (Sham, n = 5; Ti, n = 6). Data are shown as mean ± SEM (One-way ANOVA between indicated genotypes). **(H)** Representative pictures of TRAP and H&E-stained sections from the calvariae of chimeric WT and *Xaf1*^{-/-} littermates after sham and Ti particle implantation operation. Scale bar, 200 μm. **(I)** Quantification of the eroded surface area and TRAP-positive cells on sections from the calvariae of chimeric WT and *Xaf1*^{-/-} littermates after sham and Ti particle implantation operation. Data are shown as mean ± SEM (One-way ANOVA between indicated genotypes).

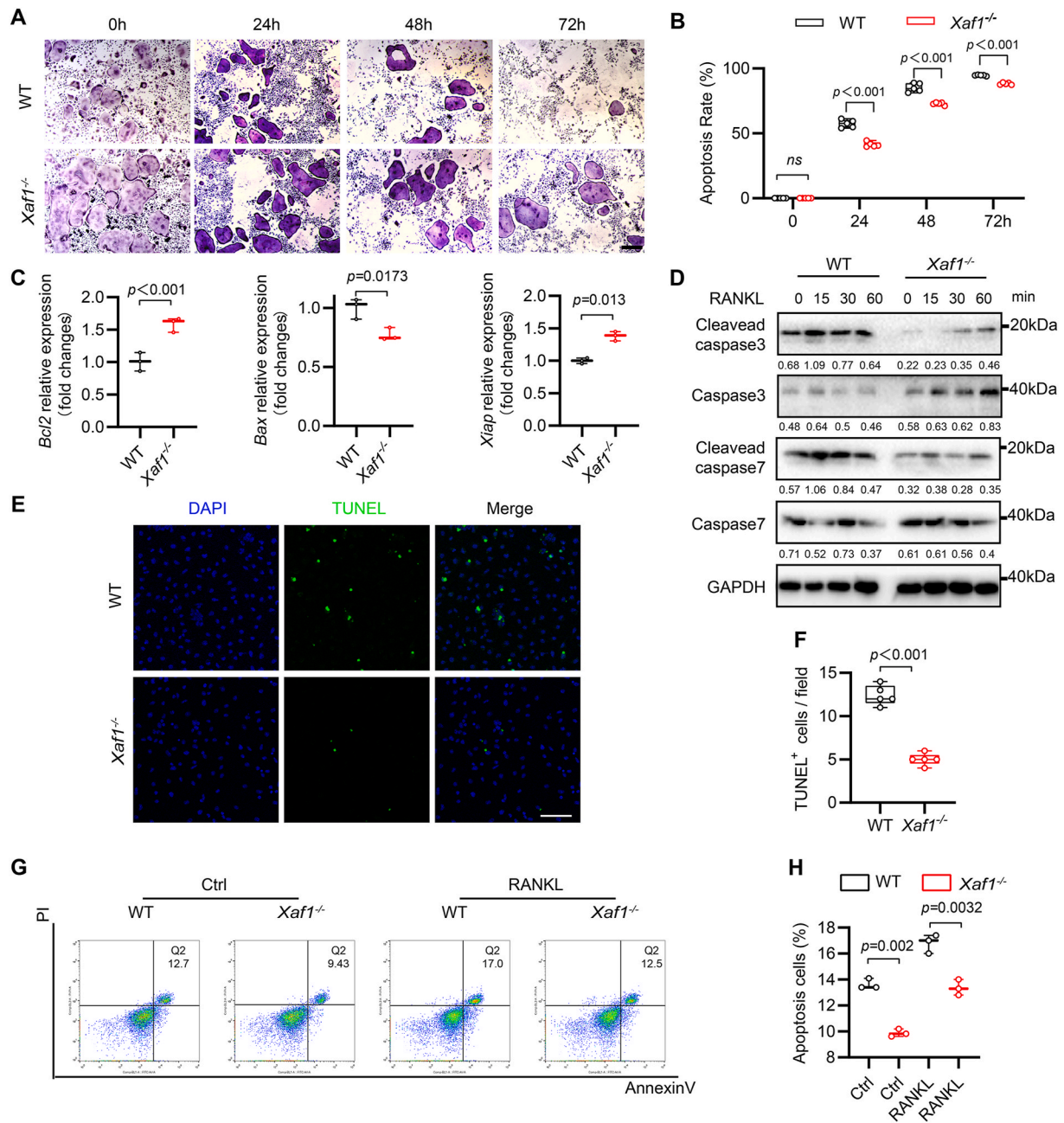


Figure 6. *Xaf1* deletion inhibits apoptosis of OCs. (A) Bone marrow cells isolated from WT and *Xaf1*^{-/-} mice were cultured on glass coverslips for 7 days in α -MEM medium supplemented with M-CSF (30 ng/ml) and RANKL (50 ng/ml). Osteoclasts were stained with TRAP at indicated time after removing cytokines. Scale bar, 50 μ m. (B) Quantification of TRAP-positive osteoclast number with a full actin ring of (A). Data are shown as mean \pm SEM (Student's *t*-test). (C) RT-qPCR analysis of the osteoclast-specific genes mRNA expression of the BMM cultures isolated from WT (*n* = 3) and *Xaf1*^{-/-} mice (*n* = 3) incubated for 3 days with M-CSF (30 ng/ml) and RANKL (50 ng/ml). Data are shown as mean \pm SEM (Student's *t*-test). (D) Western blot analysis of whole cell lysates from BMM cultures isolated from WT and *Xaf1*^{-/-} mice and stimulated with M-CSF (30 ng/ml) and RANKL (50 ng/ml) for indicated time. GAPDH is shown as a loading control. Data are representative of three independent experiments. (E) Bone marrow cells isolated from WT and *Xaf1*^{-/-} mice were cultured on glass coverslips for 3 days in α -MEM medium supplemented with M-CSF (30 ng/ml) and RANKL (50 ng/ml). On day 3, osteoclasts were stained with TUNEL. Representative images of fluorescence of TUNEL positive pre-osteoclasts. Green, TUNEL; blue, DAPI. Scale bar, 50 μ m. (F) Quantification of TUNEL positive pre-osteoclasts in (E). Data are shown as mean \pm SEM (Student's *t*-test). (G) Bone marrow cells isolated from WT and *Xaf1*^{-/-} mice were cultured on glass coverslips for 3 days in α -MEM medium supplemented with M-CSF (30 ng/ml) alone or with M-CSF and RANKL (50 ng/ml). On day 3, pre-osteoclasts were stained with Annexin V-PI using flow cytometry. (H) Quantification of apoptosis rate of pre-osteoclasts in (G). Data are shown as mean \pm SEM (One-way ANOVA between indicated genotypes).

results suggested that depletion of *Xaf1* deteriorated osteolytic bone loss by aggravating OCgenesis *in vivo*.

3.5. *Xaf1* deletion chimeras resulted in a low bone mass phenotype

In fact, global *Xaf1* deletion led to several nonskeletal pathologies,

making it challenging to distinguish between direct effects of *Xaf1* deletion on bone and secondary effects on other organs. Then, bone marrow transplantation (BMT) from the *Xaf1*^{-/-} and littermate donors was performed to generate WT mice containing macrophages deficient in *Xaf1* (*Xaf1*^{-/-}→WT) and control mice (WT→WT) (Fig. 5A). The efficiency of BMT was verified using flow cytometry (Fig. S4A). Similar

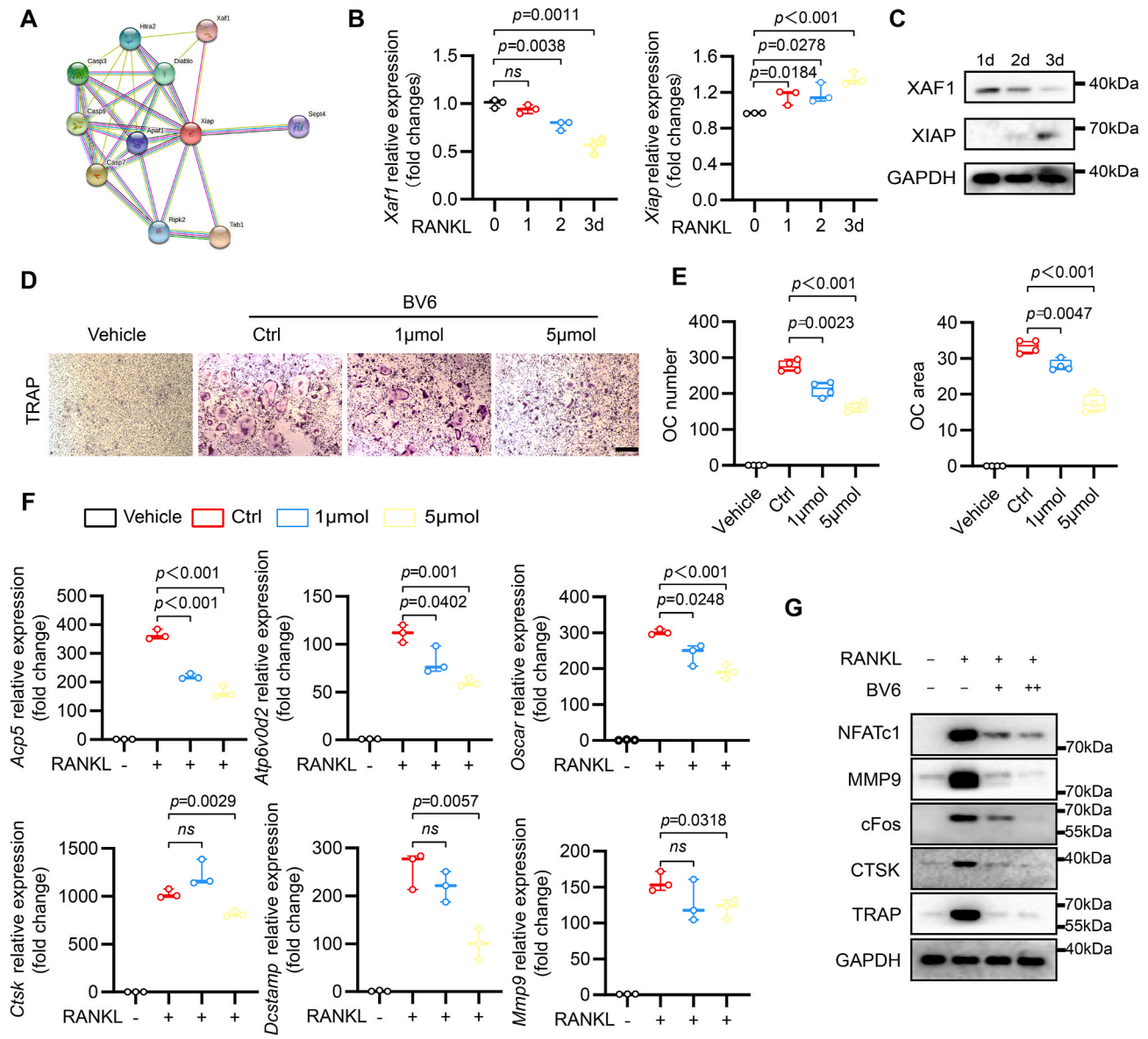


Figure 7. BV6 (XIAP inhibitor) suppresses RANKL-induced OC formation. (A) STRING analysis of XAF1 and XIAP interaction. (B) RT-qPCR analysis of the osteoclast-specific genes mRNA expression of the BMM cultures isolated from WT mice ($n = 3$) incubated for indicated time with M-CSF (30 ng/ml) and RANKL (50 ng/ml). Data are shown as mean \pm SEM (Student's *t*-test). (C) Western blot analysis of whole cell lysates from BMM cultures isolated from WT mice and stimulated with M-CSF (30 ng/ml) and RANKL (50 ng/ml) for indicated time. GAPDH is shown as a loading control. Data are representative of three independent experiments. (D) Bone marrow cells isolated from WT mice were cultured on glass coverslips for 7 days in α -MEM medium supplemented with M-CSF (30 ng/ml) and RANKL (50 ng/ml) and BV6 at indicated concentrations. On day 7, osteoclasts were stained with TRAP. Scale bar, 50 μ m. (E) Quantification of osteoclast number and percentage of osteoclast area in (D). Data are shown as mean \pm SEM (Student's *t*-test). (F) RT-qPCR analysis of the osteoclast-specific genes mRNA expression of the BMM cultures isolated from WT mice ($n = 3$) incubated for 3 days with M-CSF (30 ng/ml) and RANKL (50 ng/ml) and BV6 at indicated concentrations. Data are shown as mean \pm SEM (Student's *t*-test). (G) Western blot analysis of whole cell lysates from BMM cultures isolated from WT mice and stimulated with M-CSF (30 ng/ml) and RANKL (50 ng/ml) for indicated time and BV6 at indicated concentrations. GAPDH is shown as a loading control. Data are representative of three independent experiments.

with global deletion, *Xaf1*^{-/-} chimeric mice illustrated bone loss phenotype in OVX model (Fig. 5B). Morphometric analyses of trabecular including BV/TV, BS/TV, Tb. N and Tb.pf confirmed low bone mass in *Xaf1*^{-/-} chimeric mice (Fig. 5C). H&E and TRAP staining showed decreased bone mass, trabecular area, and increased OC number in *Xaf1*^{-/-} chimeric mice (Fig. 5D–E). Moreover, the elevated serum levels of RANKL and RANKL/OPG ratio in *Xaf1*^{-/-} chimeric mice compared to WT chimeric mice further confirmed higher bone resorption activity (Fig. S4B). No difference in serum OPG content was found between *Xaf1*^{-/-} chimeric mice and WT chimeric mice (Fig. S4B).

Meanwhile, severe bone loss in osteolysis model was observed in *Xaf1*^{-/-} chimeric mice (Fig. 5F), confirmed by morphometric (Fig. 5G)

and histological analysis (Fig. 5H), wherein an increase in the number and activity of OCs was observed (Fig. 5I). Serum levels of RANKL and RANKL/OPG ratio indicated a severe osteolytic phenotype (Fig. S4C). Both *Xaf1* global depletion and *Xaf1*^{-/-} chimeric mice generation promoted osteoclastic bone resorption in the OVX and osteolysis model. Meanwhile, *Xaf1* deletion chimeras did not affect osteogenesis, which was indicated by ELISA and RT-qPCR (Figs. S4D–E). Together, our findings demonstrated that *Xaf1* deficient in macrophages demonstrated a low-bone mass phenotype due to elevated OC number and activation.

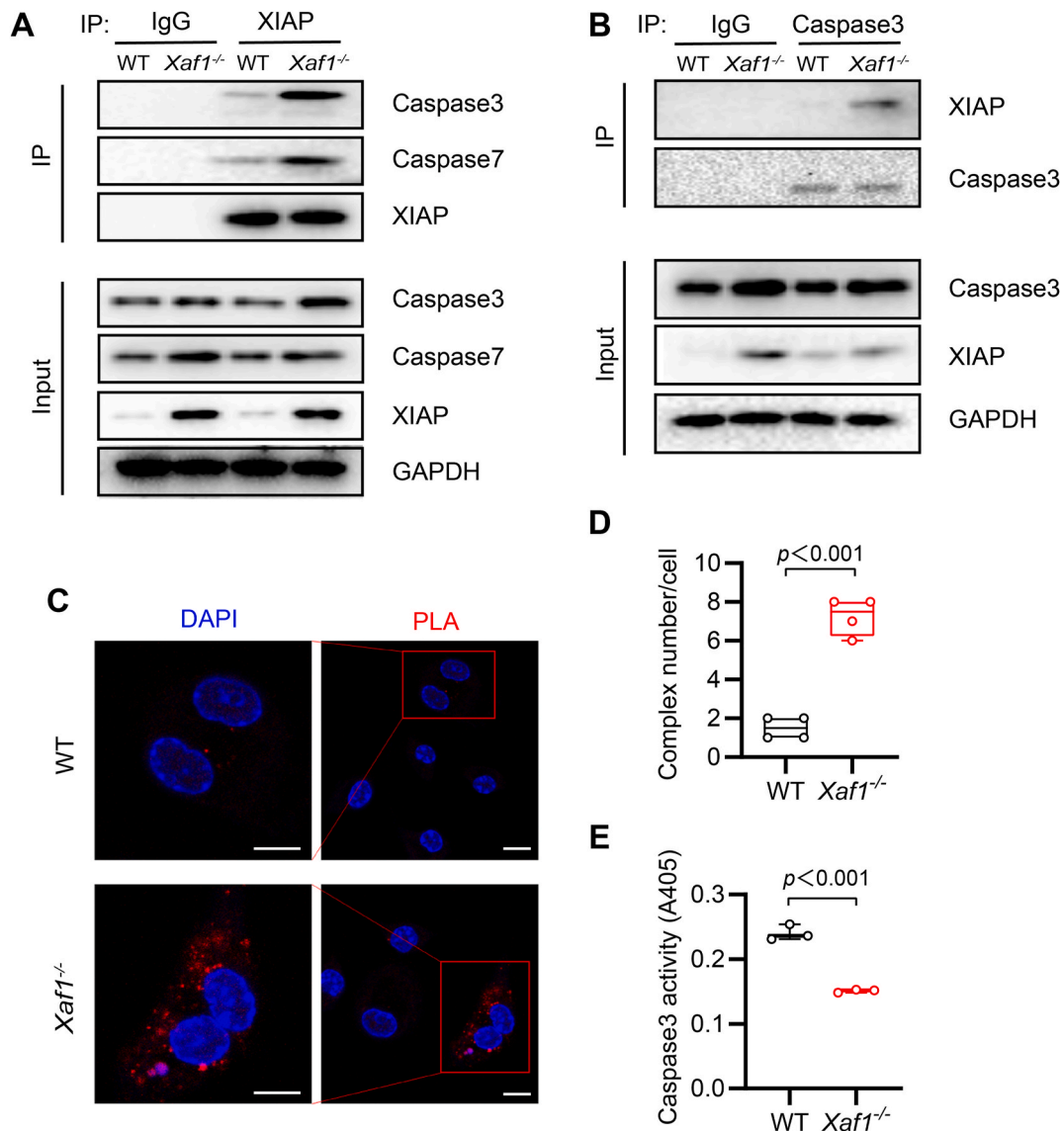


Figure 8. XAF1 interacts with XIAP to promote caspase activity. (A–B) Bone marrow cells isolated from WT and *Xaf1*^{-/-} mice were cultured on glass coverslips for 3 days in α -MEM medium supplemented with M-CSF (30 ng/ml) alone or with M-CSF (30 ng/ml) and RANKL (50 ng/ml). After lysis, XIAP and caspase3 was immunoprecipitated using an anti-XIAP and anti-caspase3 antibody, and the interaction status of caspase3 and XIAP in WT and *Xaf1*^{-/-} mice was determined by Western blotting, respectively. Data are representative of three independent experiments. (C) Bone marrow cells isolated from WT and *Xaf1*^{-/-} mice were cultured on glass coverslips for 3 days in α -MEM medium supplemented with M-CSF (30 ng/ml) and RANKL (50 ng/ml). *In situ* PLA technology indicated endogenous XIAP-caspase3 protein interactions in BMMs. Red, positive interaction complexes; blue, DAPI. Scale bar, 50 μ m. Data are representative of three independent experiments. (D) Quantification of number of positive interaction complexes of (C). Data are shown as mean \pm SEM (Student's *t*-test). (E) Caspase-3 activity assay of whole cell lysates from BMM cultures isolated from WT and *Xaf1*^{-/-} mice stimulated with M-CSF (30 ng/ml) and RANKL (50 ng/ml) for 3 days. Data are shown as mean \pm SEM (Student's *t*-test).

3.6. *Xaf1* deletion inhibited the apoptosis of OCs

Previous studies had demonstrated that mature OCs undergo spontaneous apoptosis. However, multinucleated OCs derived from *Xaf1*^{-/-} mice exhibited resistance to apoptosis due to the removal of cytokines compared with OCs derived from WT mice (Fig. 6A–B). These findings led us to examine induction of apoptosis in *Xaf1*^{-/-} OCs. Therefore, we performed RT-qPCR to determine the involvement of *Xaf1* in OC apoptosis, which confirmed downregulation of pro-apoptotic *Bax* and upregulation of anti-apoptotic *Bcl2* and *Xiap* in *Xaf1*^{-/-} cells during OCgenesis (Fig. 6C). Meanwhile, inactivation of caspase-3/7, as indicated by cleaved caspase-3/7, was also observed in BMMs derived from *Xaf1*^{-/-} mice throughout the differentiation process (Fig. 6D). When compared to the WT BMMs, *Xaf1*^{-/-} BMMs had significantly fewer cells that were positive for DNA fragmentation (TUNEL⁺) after 3 days

following RANKL stimulation, which suggested that *Xaf1*^{-/-} BMMs suppressed spontaneous apoptosis during OCgenesis (Fig. 6E–F). Flow cytometry was performed to determine OC apoptosis, indicating a decreased percentage of OC apoptosis in *Xaf1*^{-/-} BMMs treated with RANKL (Fig. 6G–H). These findings collectively suggested that *Xaf1* deficiency causes excessive OC generation via inhibiting apoptosis.

3.7. BV6 (XIAP inhibitor) suppressed RANKL-induced OC formation

Xaf1 was identified as an XIAP inhibitor gene [18,23], which was verified by STRING analysis (Fig. 7A). RT-qPCR (Fig. 7B) and western blot (Fig. 7C) analysis demonstrated that *Xaf1* experienced a complementary change with XIAP during OCgenesis. BV6, a XIAP inhibitor, was used to determine if *Xaf1* regulated OCgenesis via XIAP *in vitro*. CCK-8 assays were conducted to determine the viability of BMMs treated

with different concentrations of BV6 for 24 and 48 h, indicating that BV6 at concentrations up to 5 μ M had no discernible effect on the viability of BMMs at all time points analyzed (Fig. S5A).

To demonstrate how BV6 stimulates OCgenesis, we treated BMMs with BV6 at non-toxic concentrations for 7 days. However, a dose-dependent reduction in the number and size of OCs was observed in the BV6-treated groups (Fig. 7D), which was validated by number and area quantification of TRAP⁺ OCs (Fig. 7E). Simultaneously, RT-qPCR analyses showed that BV6 treatments dose-dependently induced the transcription of OC-specific genes in BMMs, including *Oscar*, *Dcstamp*, *Ctsk*, *Atp6v0d2*, *Mmp9*, and *Acp5* (Fig. 7F). By using total cellular proteins extracted from BMMs stimulated with BV6, we observed the dose-dependent inhibition of NFATc1, c-Fos, MMP9, CTSK and TRAP (encoded by *Acp5*) (Fig. 7G). Thus, BV6 suppressed RANKL-induced OCgenesis and inhibited OC-specific gene and protein expression in a dose-dependent manner, implying XIAP functioned as XAF1 downstream signaling to mediate OC generation and function.

3.8. XAF1 interacted with XIAP to promote the caspase-3 activity

After establishing the cellular effects of *Xaf1*, we aimed to elucidate the underlying molecular mechanism. It's been known that XIAP directly interacted with caspase and inhibits cell apoptosis. Based on these results, we hypothesized that XAF1 antagonize interaction between XIAP and caspase, thereby promoting OC apoptosis. Co-immunoprecipitation assay was performed to validate the endogenous interaction between XIAP and caspase3/7 (Fig. 8A and B). Furthermore, *in situ* proximity ligation assay (PLA) revealed a direct interaction between endogenous XIAP and caspase3 in BMMs (Fig. 8C), which confirmed by increased number of XIAP-caspase3 interaction complex (Fig. 8D). Moreover, caspase3 activity was decreased in *Xaf1*^{-/-} BMMs treated with RANKL compared to WT BMMs (Fig. 8E). These results were consistent with the effect of *Xaf1* in antagonizing XIAP-caspase interaction.

4. Discussion

In this study, XAF1 was identified as a novel bone homeostasis regulator, which suppressed RANKL-induced OCgenesis. Global or bone marrow chimera depletion of XAF1 increased the formation of OCs and led to a low-bone mass phenotype under chronic and acute conditions. Mechanistically, biochemical investigations revealed that XIAP functioned as a XAF1 interaction partner and XAF1 antagonized interaction between XIAP and caspase to mediate OC apoptosis.

XAF1 is a zinc-finger, pro-apoptotic protein that is originally identified in a yeast two-hybrid screen utilizing XIAP as the bait [18]. Because of abnormal promoter methylation and gene silencing, XAF1 expression is commonly inactivated in human malignancies, implicating XAF1 in tumor suppression [24]. XAF1 is involved in pancreatic, breast, and prostate cancer by inhibiting cell apoptosis [25–27]. However, the role of XAF1 in osteoporosis and bone remodeling has been unknown. Here, we determined that XAF1 was present in OCs and played an essential role in OCgenesis and bone resorption *in vitro* and *in vivo*. Our *Xaf1* global deletion and bone marrow chimera animals showed osteoporotic and osteolytic low-bone mass phenotypes. Meanwhile, our study was the first to document that increased OC generation and bone resorption *in vivo* was the source of the osteoporotic phenotype brought on by the loss of *Xaf1*. Based on its significant role in shortening the lifespan of OCs, XAF1, as a protective molecule, played a critical role in the maintenance of bone homeostasis.

Apoptosis is related with several diseases, including cancer, neurodegenerative, and autoimmune diseases, such as rheumatoid arthritis (RA). Studies have shown that the decrease in cell apoptosis could lead to the accumulation of inflammatory cells and OCs in the synovial joints [28,29]. Apoptosis induction inhibits synovial inflammation and bone erosion, demonstrating potential therapeutic effects in RA patients and

mice [30]. Moreover, attenuation in the apoptosis of OC causes bone loss in postmenopausal women with OP since estrogen deficiency decreases pro-apoptotic ligand FasL expression [22]. Furthermore, bisphosphonates are effective anti-resorptive drugs for treating patients with OP and promoting the apoptosis of OCs [31]. These results indicate a close correlation between OC lifespan and the pathogenesis of bone metabolic diseases. Hence, targeting osteoclastic apoptosis in affected patients could be helpful for halting bone loss.

Inhibitor of apoptosis proteins (IAP) are the only endogenous proteins regulating the initiation and effector activity of cysteine proteases [32], which are associated with apoptosis [33]. IAPs, including XIAP, inhibits the activation of caspases and intrinsically regulates the caspase signaling pathway. XAF1, identified as XIAP inhibitor, induces nuclear translocation and antagonizes anti-trypsin activity of XIAP [18], which was consistent with our results, indicating that XAF1 and XIAP expression exhibited contrast changes under RANKL stimulation. Combining anti-tumor function with our findings, *Xaf1* may be under strict transcriptional regulation to prevent abnormal cellular behavior and *Xaf1* deletion prolonged OC survival by exerting anti-apoptotic effects [25]. Notably, XAF1 is a crucial regulator of OC-mediated bone homeostasis through apoptosis.

Studies initially focus on the capacity of XIAP to bind to and inhibit caspases that control apoptotic cell death [34]. Proapoptotic caspases are proteases that break down cells, thus they need to be carefully managed to avoid either uncontrolled cell death or the unintended survival of damaged or cancerous cells. A linker region between BIR domains 1 and 2 is where XIAP interacts to caspases 3 and 7 in apoptotic signaling [35]. Our discovery that XAF1 mediated the activity of caspase 3 and the interaction between XIAP and caspase3/7 may offer new insights into how OCgenesis could be precisely adjusted and controlled during pathological osteoporosis, which shifts the balance from normalcy towards apoptosis. Besides, it's interesting to note that the lengthy 5' and 3' UTRs on the XIAP transcript may allow for independent regulation of XIAP protein levels from transcriptional regulation of the mRNA. The human XIAP 5' UTR has an internal ribosome entry site (IRES) region that enables XIAP production in stressed cells even if cap-dependent translation is normally blocked [36]. As a result, under the same stress circumstances, XIAP protein may be preferentially up-regulated in comparison to other cellular proteins [37], which supported for the effect of BV6 on OCgenesis in our study.

The Bcl2 family is involved in OC apoptosis and affects the survival of osteocytes and osteoblasts [38]. Therefore, reducing the threshold of OC apoptosis could aid in developing new targeted therapies for patients with bone loss. Our results showed that *Xaf1* could affect the production and functions of OCs, but did not significantly affect osteoblasts *in vitro* and *in vivo* (Fig. S2). XAF1 induces intrinsic cell apoptosis by promoting Bax expression and inhibiting Bcl2 expression mediated by p53 and cAMP response element-binding protein, respectively [39,40], which in accordance with our results, demonstrating an increase in the mRNA expression levels of several apoptosis-related genes in OCs derived from *Xaf1* deletion mice. Therefore, XAF1 plays an essential role in OC apoptosis.

In fact, multiple XAF1 transcripts, including full-length (XAF1A) and short truncated (XAF1B-E), are expressed via alternative splicing in normal human tissues [41,42]. Recent study has shown the crosstalk between bone and other organs [43]. Hence, the effect of XAF1 activation in the liver or other organs on bone health cannot be ignored. Based on this, bone marrow transplantation was performed to construct chimeric mice to mimic deletion of *Xaf1* expression in macrophages. If permitted, bisphosphonates or denosumab can be utilized to rescue low-bone mass phenotype, validating the bone-dependent mechanism. However, inconsistent with our findings of RNA-seq, *Xaf1* played a protective role in OCgenesis. From our perspective, inflammatory microenvironment of osteoporosis led to the increase of *Xaf1* transcript factor, such as *Irf1* and *Stat1*, enhancing *Xaf1* expression. Meanwhile, XAF1 functioned as an osteoprotective factor and its up-regulation

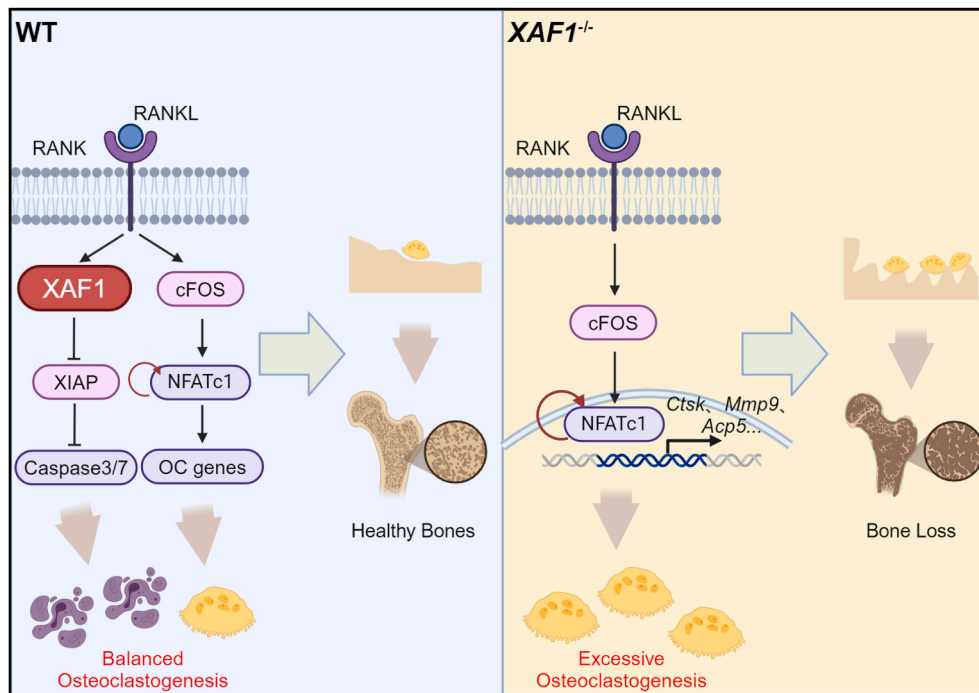


Figure 9. Schematic model depicting the role of XAF1 in regulating osteoclastogenesis.

prevented over-activated OCgenesis and excessive bone loss [44–46], which was indicated by deteriorative osteopenia phenotype in *Xaf1*^{-/-} mice treated with OVX and Ti-particle.

Some limitations of our study should also be mentioned here. First, there had been several literature reports confirming the role of *Xaf1* in antiviral immunity, diabetes, and cancers [25,47,48] hence global *Xaf1* knockout may have an indirect effect on bone phenotype. Although bone marrow transplantation could largely mimic the effect of conditional knockout of myeloid cells, thereby eliminating the indirect effects of other organs on bone as much as possible, it would be more informative to explore the effect of XAF1 on osteoclastogenesis via a conditional knock out in osteoclast. Second, XAF1 expression was at low level under physiological conditions and only increased under the stimulation of inflammatory environment such as virus infection [16,18,49]. Therefore, we believed that the expression level of XAF1 under physiological conditions was insufficient to produce a distinct bone phenotype and that was why the number of sham group was not comparable with that of operation group in OVX and osteolysis model. Third, our study has proved that XAF1 was involved in bone metabolism, especially in OCgenesis rather than osteogenesis. Although we have clarified the role of XAF1 in OC apoptosis, unaffected osteogenesis pattern should be elucidated. In fact, bone homeostasis and microenvironment consist of OC, osteoblast and other immune cells [50]. XAF1 has exhibited its significance in immune microenvironment and tumorigenesis [51]. Whether XAF1 has an indirect influence on osteoblast by other bone cells or immune cells remains unclear, which prompts us to explore in the further research.

In conclusion, our study demonstrated that *Xaf1* promoted OC apoptosis via the XIAP-Caspase-3/7 signaling pathway, thereby inhibiting OC formation and function (Fig. 9). To the best of our knowledge, our study is the first to demonstrate that *Xaf1* deletion could enhance OCgenesis by inhibiting cell apoptosis. Our results could shed light on the role of *Xaf1* in bone homeostasis and targeting *Xaf1* may be beneficial as a therapeutic approach.

Declaration of interests

None.

CRediT authorship contribution statement

Mingchao Zhang: Data curation, Investigation, Methodology, Writing – original draft. **Yingkang Huang:** Investigation, Methodology, Writing – review & editing. **Jinyu Bai:** Investigation, Methodology. **Wushuang Xu:** Investigation, Methodology. **Huajian Shan:** Writing – review & editing. **Lei Sheng:** Writing – review & editing. **Xiang Gao:** Writing – review & editing. **Yu Han:** Investigation. **Shiyong Wang:** Investigation. **Chaowen Bai:** Investigation, Writing – review & editing, Investigation. **Bo Tian:** Writing – review & editing. **Yichao Ni:** Writing – review & editing. **Qirong Dong:** Funding acquisition, Supervision. **Feng Ma:** Conceptualization, Funding acquisition, Supervision, Writing – review & editing. **Xiaozhong Zhou:** Conceptualization, Supervision, Funding acquisition, Writing – original draft, Writing – review & editing.

Acknowledgments

We would like to sincerely thank Jiangsu Provincial Medical Key Discipline (Laboratory) for the platform and technical assistance. This study was funded by the National Key Research and Development Program of China (2018YFA0900803), National Natural Science Foundation of China (Grant No. 82172425, 81974334), Natural Science Foundation of Jiangsu Province (BK20200004), Jiangsu Provincial Medical Key Discipline (Grant No. JSEMW202223), Postgraduate Research & Practice Innovation Program of Jiangsu Province (Grant No. KYCX223222), CAMS Innovation Fund for Medical Sciences (2021-I2M-1-047 and 2022-I2M-2-004), and the Special Research Fund for Central Universities, Peking Union Medical College (3332022160).

Appendix A. Supplementary data

Supplementary data to this article can be found online at <https://doi.org/10.1016/j.jot.2024.05.001>.

Under RANKL stimulation, in the presence of XAF1, osteoclasts went through differentiation and apoptosis to maintain controlled bone metabolism. On the other hand, XAF1 depletion inhibited osteoclast apoptosis via the XIAP-Caspase-3/7 signaling pathway, thus enhancing osteoclastogenesis and leading to bone loss.

References

- [1] Rachner T, Khosla S, Hofbauer. Osteoporosis: now and the future. *Lancet* 2011;377(9773):1276–87. [https://doi.org/10.1016/s0140-6736\(10\)62349-5](https://doi.org/10.1016/s0140-6736(10)62349-5).
- [2] Kobayashi Y, Uehara S, Udagawa N, Takahashi N. Regulation of bone metabolism by Wnt signals. *Journal of biochemistry* 2016;159(4):387–92. <https://doi.org/10.1093/jb/mvv124>.
- [3] Reid I, Billington E. Drug therapy for osteoporosis in older adults. *Lancet* 2022;399(10329):1080–92. [https://doi.org/10.1016/s0140-6736\(21\)02646-5](https://doi.org/10.1016/s0140-6736(21)02646-5).
- [4] Tsukasaki M, Takayanagi H. Osteoimmunology: evolving concepts in bone-immune interactions in health and disease. *Nat Rev Immunol* 2019;19(10):626–42. <https://doi.org/10.1038/s41577-019-0178-8>.
- [5] Fischer V, Haffner-Luntzer M. Interaction between bone and immune cells: implications for postmenopausal osteoporosis. *Semin Cell Dev Biol* 2022;123:14–21. <https://doi.org/10.1016/j.semcdb.2021.05.014>.
- [6] Guder C, Gravius S, Burger C, Wirtz D, Osteoimmunology Schildberg. A current update of the interplay between bone and the immune system. *Front Immunol* 2020;11:58. <https://doi.org/10.3389/fimmu.2020.00058>.
- [7] Negishi-Koga T, Takayanagi. Bone cell communication factors and Semaphorins. *BoneKey Rep* 2012;1:183. <https://doi.org/10.1038/bonekey.2012.183>.
- [8] Theill L, Boyle W, Penninger J. RANK-L and RANK: T cells, bone loss, and mammalian evolution. *Annu Rev Immunol* 2002;20:795–823. <https://doi.org/10.1146/annurev.immunol.20.100301.064753>.
- [9] Meednu N, Zhang H, Owen T, Sun W, Wang V, Cistrone C, et al. Production of RANKL by memory B cells: a link between B cells and bone erosion in rheumatoid arthritis. *Arthritis Rheumatol* 2016;68(4):805–16. <https://doi.org/10.1002/art.39489>.
- [10] Srivastava R, Dar H, Mishra P. Immunoporosis: immunology of osteoporosis-role of T cells. *Front Immunol* 2018;9:657. <https://doi.org/10.3389/fimmu.2018.00657>.
- [11] Woo S, Corrales L, Gajewski T. Innate immune recognition of cancer. *Annu Rev Immunol* 2015;33:445–74. <https://doi.org/10.1146/annurev-immunol-032414-112043>.
- [12] Takayanagi H, Kim S, Matsuo K, Suzuki H, Suzuki T, Sato K, et al. RANKL maintains bone homeostasis through c-Fos-dependent induction of interferon-beta. *Nature* 2002;416(6882):744–9. <https://doi.org/10.1038/416744a>.
- [13] Zhao B, Takami M, Yamada A, Wang X, Koga T, Hu X, et al. Interferon regulatory factor-8 regulates bone metabolism by suppressing osteoclastogenesis. *Nat Med* 2009;15(9):1066–71. <https://doi.org/10.1038/nm.2007>.
- [14] Leaman D, Chawla-Sarkar M, Vyas K, Reheman M, Tamai K, Toji S, et al. Identification of X-linked inhibitor of apoptosis-associated factor-1 as an interferon-stimulated gene that augments TRAIL Apo2L-induced apoptosis. *J Biol Chem* 2002;277(32):28504–11. <https://doi.org/10.1074/jbc.M204851200>.
- [15] Leaman D, Chawla-Sarkar M, Jacobs B, Vyas K, Sun Y, Ozdemir A, et al. Novel growth and death related interferon-stimulated genes (ISGs) in melanoma: greater potency of IFN-beta compared with IFN-alpha2. *J Interferon Cytokine Res* 2003;23(12):745–56. <https://doi.org/10.1089/107999003772084860>.
- [16] Han Y, Bai X, Liu S, Zhu J, Zhang F, Xie L, et al. XAF1 protects host against emerging RNA viruses by stabilizing IRF1-dependent antiviral immunity. *J Virol* 2022;96(17):e0077422. <https://doi.org/10.1128/jvi.00774-22>.
- [17] Fong W, Liston P, Rajcan-Separovic E, St Jean M, Craig C, Korneluk R. Expression and genetic analysis of XIAP-associated factor 1 (XAF1) in cancer cell lines. *Genomics* 2000;70(1):113–22. <https://doi.org/10.1006/geno.2000.6364>.
- [18] Liston P, Fong W, Kelly N, Toji S, Miyazaki T, Conte D, et al. Identification of XAF1 as an antagonist of XIAP anti-Caspase activity. *Nat Cell Biol* 2001;3(2):128–33. <https://doi.org/10.1038/35055027>.
- [19] Tanaka S, Miyazaki T, Fukuda A, Akiyama T, Kadono Y, Wakeyama H, et al. Molecular mechanism of the life and death of the osteoclast. *Ann N Y Acad Sci* 2006;1068:180–6. <https://doi.org/10.1196/annals.1346.020>.
- [20] Wang S, Deng Z, Ma Y, Jin J, Qi F, Li S, et al. The role of autophagy and mitophagy in bone metabolic disorders. *Int J Biol Sci* 2020;16(14):2675–91. <https://doi.org/10.7150/ijbs.46627>.
- [21] Chamoux E, Houde N, L'Eriger K, Roux S. Osteoprotegerin decreases human osteoclast apoptosis by inhibiting the TRAIL pathway. *J Cell Physiol* 2008;216(2):536–42. <https://doi.org/10.1002/jcp.21430>.
- [22] Nakamura T, Imai Y, Matsumoto T, Sato S, Takeuchi K, Igarashi K, et al. Estrogen prevents bone loss via estrogen receptor alpha and induction of Fas ligand in osteoclasts. *Cell* 2007;130(5):811–23. <https://doi.org/10.1016/j.cell.2007.07.025>.
- [23] Siegelin M, Touzani O, Toutain J, Liston P, Rami A. Induction and redistribution of XAF1, a new antagonist of XIAP in the rat brain after transient focal ischemia. *Neurobiol Dis* 2005;20(2):509–18.
- [24] Plenchette S, Cheung H, Fong W, LaCasse E, Korneluk R. The role of XAF1 in cancer. *Curr Opin Invest Drugs* 2007;8(6):469–76.
- [25] Nishimura Y, Iwashita M, Hayashi M, Shinjo T, Watanabe Y, Zeze T, et al. XAF1 overexpression exacerbates diabetes by promoting pancreatic beta-cell apoptosis. *Acta Diabetol* 2022;59(10):1275–86. <https://doi.org/10.1007/s00592-022-01930-y>.
- [26] Lim J-S, Lee K-W, Ko K-P, Jeong S-I, Ryu B-K, Lee M-G, et al. XAF1 destabilizes estrogen receptor alpha through the assembly of a BRCA1-mediated destruction complex and promotes estrogen-induced apoptosis. *Oncogene* 2022;41(20):2897–908. <https://doi.org/10.1038/s41388-022-02315-9>.
- [27] Camacho-Moctezuma B, Quevedo-Castillo M, Melendez-Zajjala J, Aquino-Jarquín G, Martínez-Ruiz GU. YY1 negatively regulates the XAF1 gene expression in prostate cancer. *Biochem Biophys Res Commun* 2019;508(3):973–9. <https://doi.org/10.1016/j.bbrc.2018.12.056>.
- [28] Zhao J, Jiang P, Guo S, Schrodi SJ, He D. Apoptosis, autophagy, NETosis, necroptosis, and pyroptosis mediated programmed cell death as targets for innovative therapy in rheumatoid arthritis. *Front Immunol* 2021;12:809806. <https://doi.org/10.3389/fimmu.2021.809806>.
- [29] Dharmapatri A, Smith M, Findlay D, Holding C, Evdokiou A, Ahern M, et al. Elevated expression of caspase-3 inhibitors, survivin and XIAP correlates with low levels of apoptosis in active rheumatoid synovium. *Arthritis Res Ther* 2009;11(1):R13. <https://doi.org/10.1186/ar2603>.
- [30] Dharmapatri AASSK, Cantley MD, Marino V, Perilli E, Crotti TN, Smith MD, et al. The X-linked inhibitor of apoptosis protein inhibitor embelin suppresses inflammation and bone erosion in collagen antibody induced arthritis mice. *Mediat Inflamm* 2015;2015:564042. <https://doi.org/10.1155/2015/564042>.
- [31] Weinstein R, Manolagas S. Apoptosis and osteoporosis. *Am J Med* 2000;108(2):153–64. [https://doi.org/10.1016/s0002-9343\(99\)00420-9](https://doi.org/10.1016/s0002-9343(99)00420-9).
- [32] Holcik M, Gibson H, Korneluk R. XIAP: apoptotic brake and promising therapeutic target. *Apoptosis* 2001;6(4):253–61. <https://doi.org/10.1023/a:1011379307472>.
- [33] Hunter A, LaCasse E, Korneluk R. The inhibitors of apoptosis (IAPs) as cancer targets. *Apoptosis* 2007;12(9):1543–68. <https://doi.org/10.1007/s10495-007-0087-3>.
- [34] Scott F, Denault J, Riedl S, Shin H, Renatus M, Salvesen G. XIAP inhibits caspase-3 and -7 using two binding sites: evolutionarily conserved mechanism of IAPs. *EMBO J* 2005;24(3):645–55. <https://doi.org/10.1038/sj.emboj.7600544>.
- [35] Wilkinson J, Cepero E, Boise L, Duckett C. Upstream regulatory role for XIAP in receptor-mediated apoptosis. *Mol Cell Biol* 2004;24(16):7003–14. <https://doi.org/10.1128/mcb.24.16.7003-7014.2004>.
- [36] Holcik M, Lefebvre C, Yeh C, Chow T, Korneluk R. A new internal-ribosome-entry-site motif potentiates XIAP-mediated cytoprotection. *Nat Cell Biol* 1999;1(3):190–2. <https://doi.org/10.1038/11109>.
- [37] Holcik M, Korneluk R. Functional characterization of the X-linked inhibitor of apoptosis (XIAP) internal ribosome entry site element: role of La autoantigen in XIAP translation. *Mol Cell Biol* 2000;20(13):4648–57. <https://doi.org/10.1128/mcb.20.13.4648-4657.2000>.
- [38] Komori T. Functions of the osteocyte network in the regulation of bone mass. *Cell Tissue Res* 2013;352(2):191–8. <https://doi.org/10.1007/s00441-012-1546-x>.
- [39] Tan J, Zhuang L, Leong H-S, Iyer NG, Liu ET, Yu Q. Pharmacologic modulation of glycogen synthase kinase-3beta promotes p53-dependent apoptosis through a direct Bax-mediated mitochondrial pathway in colorectal cancer cells. *Cancer Res* 2005;65(19):9012–20.
- [40] Lonze BE, Ginty DD. Function and regulation of CREB family transcription factors in the nervous system. *Neuron* 2002;35(4):605–23.
- [41] Chung S, Lee M, Ryu B, Lee J, Han J, Byun D, et al. Frequent alteration of XAF1 in human colorectal cancers: implication for tumor cell resistance to apoptotic stresses. *Gastroenterology* 2007;132(7):2459–77. <https://doi.org/10.1053/j.gastro.2007.04.024>.
- [42] Yin W, Cheepala S, Clifford J. Identification of a novel splice variant of X-linked inhibitor of apoptosis-associated factor 1. *Biochem Biophys Res Commun* 2006;339(4):1148–54. <https://doi.org/10.1016/j.bbrc.2005.11.128>.
- [43] Lu K, Shi T-S, Shen S-Y, Shi Y, Gao H-L, Wu J, et al. Defects in a liver-bone axis contribute to hepatic osteodystrophy disease progression. *Cell Metab* 2022;34(3):441–57.e7. <https://doi.org/10.1016/j.cmet.2022.02.006>.
- [44] Henning P, Movérare-Skrtic S, Westerlund A, Chaves de Souza P, Floriano-Marcelino T, Nilsson K, et al. WNT16 is robustly increased by oncostatin M in mouse calvarial osteoblasts and acts as a negative feedback regulator of osteoclast formation induced by oncostatin M. *J Inflamm Res* 2021;14:4723–41. <https://doi.org/10.2147/jir.S323435>.
- [45] Kim J, Kim K, Jin H, Song I, Youn B, Lee S, et al. Negative feedback control of osteoclast formation through ubiquitin-mediated down-regulation of NFATc1. *J Biol Chem* 2010;285(8):5224–31. <https://doi.org/10.1074/jbc.M109.042812>.
- [46] Du J, Liu Y, Wu X, Sun J, Shi J, Zhang H, et al. BRD9-mediated chromatin remodeling suppresses osteoclastogenesis through negative feedback mechanism. *Nat Commun* 2023;14(1):1413. <https://doi.org/10.1038/s41467-023-37116-5>.
- [47] Kuang M, Zhao Y, Yu H, Li S, Liu T, Chen L, et al. XAF1 promotes anti-RNA virus immune responses by regulating chromatin accessibility. *Sci Adv* 2023;9(33):eadg5211. <https://doi.org/10.1126/sciadv.adg5211>.
- [48] Lee M-G, Choi Z, Lim N-J, Lim J-S, Lee K-W, Ko K-P, et al. XAF1 directs glioma response to temozolomide through apoptotic transition of autophagy by activation of ATM-AMPK signaling. *Neurooncol Adv* 2022;4(1):vdac013. <https://doi.org/10.1093/onoajnl/vdac013>.
- [49] Liu B-Q, Liu R-B, Li W-P, Mao X-T, Li Y-N, Huang T, et al. XAF1 prevents hyperproduction of type I interferon upon viral infection by targeting IRF7. *EMBO Rep* 2023;24(1):e55387. <https://doi.org/10.15252/embr.202255387>.
- [50] Kular J, Tickner J, Chim SM, Xu J. An overview of the regulation of bone remodelling at the cellular level. *Clin Biochem* 2012;45(12):863–73. <https://doi.org/10.1016/j.clinbiochem.2012.03.021>.
- [51] Chen M, Wang K, Han Y, Yan S, Yuan H, Liu Q, et al. Identification of XAF1 as an endogenous AKT inhibitor. *Cell Rep* 2023;42(7):112690. <https://doi.org/10.1016/j.celrep.2023.112690>.